Journal of
Manufacturing and Materials Processing

MDPI

Article

Experimental and Machine Learning Study on Friction Stir Surface Alloying in Al1050-Cu Alloy

Siamak Pedrammehr [1], Moosa Sajed [2], Kais I. Abdul-Lateef Al-Abdullah [3], Sajjad Pakzad [1,*], Ahad Zare Jond [1], Mohammad Reza Chalak Qazani [4] and Mir Mohammad Ettefagh [5]

1 Faculty of Design, Tabriz Islamic Art University, Tabriz 5164736931, Iran; s.pedrammehr@tabriziau.ac.ir (S.P.); a.zare@tabriziau.ac.ir (A.Z.J.)
2 Mechanical Engineering Department, Azarbaijan Shahid Madani University, Tabriz 4691187819, Iran; sajed@azaruniv.ac.ir
3 Department of Electrical Engineering, Australian University (AU), Mubarak Al-Kabeer 1411, Kuwait; k.alabdullah@au.edu.kw
4 Faculty of Computing and Information Technology (FoCIT), Sohar University, Sohar 311, Oman; mqazani@su.edu.om
5 Faculty of Mechanical Engineering, University of Tabriz, Tabriz 5166616471, Iran; ettefagh@tabrizu.ac.ir
* Correspondence: s.pakzad@tabriziau.ac.ir

Abstract: This study employs friction stir processing to create a surface alloy using Al1050 aluminum as the base material, with Cu powder applied to enhance surface properties. Various parameters, including tool rotation speed, feed rate, and the number of passes, are investigated for their effects on the microstructure and mechanical properties of the resulting surface alloy. The evaluation methods include tensile testing, microhardness measurements, and metallographic examinations. The initial friction stir alloying pass produced a non-uniform stir zone, which was subsequently homogenized with additional passes. Through the plasticization of Al1050, initial agglomerates of copper particles were compacted into larger ones and saturated with aluminum. The alloyed samples exhibited up to an 80% increase in the strength of the base metal. This significant enhancement is attributed to the Cu content and grain size refinement post-alloying. Additionally, machine learning techniques, specifically Genetic Programming, were used to model the relationship between processing parameters and the mechanical properties of the alloy, providing predictive insights for optimizing the surface alloying process.

Keywords: friction stir surface alloying; aluminum 1050; copper powder; machine learning; genetic programming

Citation: Pedrammehr, S.; Sajed, M.; Al-Abdullah, K.I.A.-L.; Pakzad, S.; Zare Jond, A.; Chalak Qazani, M.R.; Ettefagh, M.M. Experimental and Machine Learning Study on Friction Stir Surface Alloying in Al1050-Cu Alloy. *J. Manuf. Mater. Process.* **2024**, *8*, 163. https://doi.org/10.3390/jmmp8040163

Academic Editor: Dulce Maria Rodrigues

Received: 24 June 2024
Revised: 25 July 2024
Accepted: 25 July 2024
Published: 30 July 2024

1. Introduction

The technology known as Friction Stir Processing (FSP) has garnered significant attention and research interest, particularly in its application to aluminum-based alloys, composites, and copper alloys [1,2]. FSP offers a solid-state approach to enhancing the microstructure and mechanical properties of metals, including the incorporation of various elements such as SiC powder, akin to other solid-state thermomechanical processes [3]. The development of materials that improve durability through the combination of high strength and toughness has presented significant challenges. Nevertheless, high-strength aluminum alloys have become more widely embraced due to their high strength-to-weight ratio, making them suitable for constructing lightweight structures [4]. Modern aluminum alloys are extensively utilized in various structural components within the aviation and automotive industries because of their advantageous characteristics, such as a high power-to-weight ratio, affordability, and superior wear resistance. To further broaden their application scope, it is crucial to employ straightforward and cost-effective manufacturing techniques for producing the majority of aluminum alloys. By integrating reinforcements and enhancements in the form of aluminum compounds, silicon carbide, graphite, powdered

compounds, and other materials, the base alloy of aluminum can be easily modified using inexpensive casting and mixing methods [5]. Copper is one of the main elements in the alloying of aluminum alloys. Alloys rich in copper were developed and gained substantial popularity in the commercial sector, primarily in the United States during the 1990s. These alloys were notably utilized in projects such as the External Super Lightweight Tank of the Space Shuttle and the F-16 fighter aircraft [6]. Successful demonstrations of producing metal matrix composites (MMCs) reinforced with aluminum using FSP have been reported, showcasing its potential [1].

Extensive research has been conducted on FSP, revealing its capability to improve the properties of different alloys. For instance, in aluminum alloys, FSP significantly refines the grain structure, leading to enhanced mechanical properties. Chainarong et al. [7] observed increased hardness and tensile strength properties in SSM 356 aluminum alloys processed using FSP. Similarly, FSP has shown positive effects on the microstructure and material properties in copper alloys, as demonstrated by Hasan et al. [2], who explored the formation of graphene-stabilized zero-valent copper nanoparticles in situ. Furthermore, the microstructure of materials undergoes significant changes when subjected to FSP and Friction Stir Welding (FSW). Liu et al. [8] examined the microstructure of a friction stir welded 6061 aluminum alloy, highlighting distinct alterations induced by FSP and FSW. Overall, the literature supports the effectiveness of FSP and FSW in enhancing the microstructure and mechanical properties of aluminum and copper alloys [2,7–9], offering potential benefits for various applications, including the automotive industry, where aluminum usage is increasing. However, further research is necessary to optimize process parameters and understand the fatigue behavior of dissimilar friction stir welds between different alloys [10].

Researchers have widely employed SiC and alumina (Al_2O_3) to reinforce aluminum alloys using FSP. Shafiei-Zarghani et al. [11] incorporated nano-sized Al_2O_3 particles into an AA6082 aluminum alloy through FSP, resulting in a particulate composite surface layer. Huang and Aoh [12] proposed a novel FSP technique involving the incorporation of copper-coated SiC particulate reinforcement into an Al6061 alloy matrix. Similarly, Sharma et al. [13] studied the development of hybrid surface aluminum matrix composites through FSP, identifying distinct material flow patterns. Friction Stir Alloying (FSA) is another promising technique in materials science and engineering, involving the use of FSW to introduce alloying elements into a base material, enhancing its mechanical properties. Studies have investigated the effects of different alloying elements on the microstructure and mechanical properties of FSA joints [14,15]. Despite its advantages, such as reduced porosity and improved joint strength compared to conventional fusion welding techniques, FSA faces challenges related to achieving a uniform distribution of alloying elements throughout the joint region. Nonetheless, it holds promise for various applications in industries such as automotive, aerospace, and marine engineering, with further research needed to optimize process parameters and overcome existing limitations for widespread industrial adoption.

Machine learning provides a robust framework for analyzing complex datasets and revealing intricate relationships between process parameters and material characteristics, thereby facilitating more precise predictions in Friction Stir Processing (FSP) applications [16]. Verma et al. [17] examined the utility of machine learning approaches in modeling the friction stir welding of an aviation-grade aluminum alloy, demonstrating their potential to advance understanding and prediction within this specific welding process. Additionally, Chadha et al. [18] conducted a comprehensive survey on the application of machine learning in friction stir welding, addressing current advancements, unresolved issues, and future research directions in this domain. Moreover, Anandan and Manikandan [19] employed various regression models integrated with the K-Fold cross-validation method to predict the ultimate tensile strength of friction stir welded AA 2050-T8 joints. Acharya and Mandal [20] investigated the microstructure of a friction stir processed hypereutectic Al-20Si alloy and analyzed its wear behavior using machine learning algorithms,

aiming to discern the correlation between microstructure and wear properties. Elsheikh [21] explored diverse applications of machine learning in friction stir welding, such as predicting joint properties, real-time control, and tool failure diagnosis, highlighting its potential to enhance the efficiency and effectiveness of friction stir welding processes.

In the present study, friction stir alloying was employed to create a surface alloy. The base material used was Al1050 aluminum alloy, where Cu powder was introduced onto the aluminum surface. The research focused on investigating the impact of various parameters, including tool rotation speed (1250 and 630 rpm), feed rate (20, 50, and 80 mm/min), and the number of passes (1, 3, and 6 passes) on the microstructure and mechanical properties of the resulting surface alloys. The evaluation of the samples involved conducting tensile tests, measuring microhardness, and performing metallographic examinations using optical microscopy. The machine learning technique is also applied to model the relation between the processing parameters and mechanical properties of the alloy using Genetic Programming (GP) methodology. Developing this model makes it possible to predict the mechanical properties of the designed alloy without the need to do any experiments. Figure 1 shows the graphical representation of the current research.

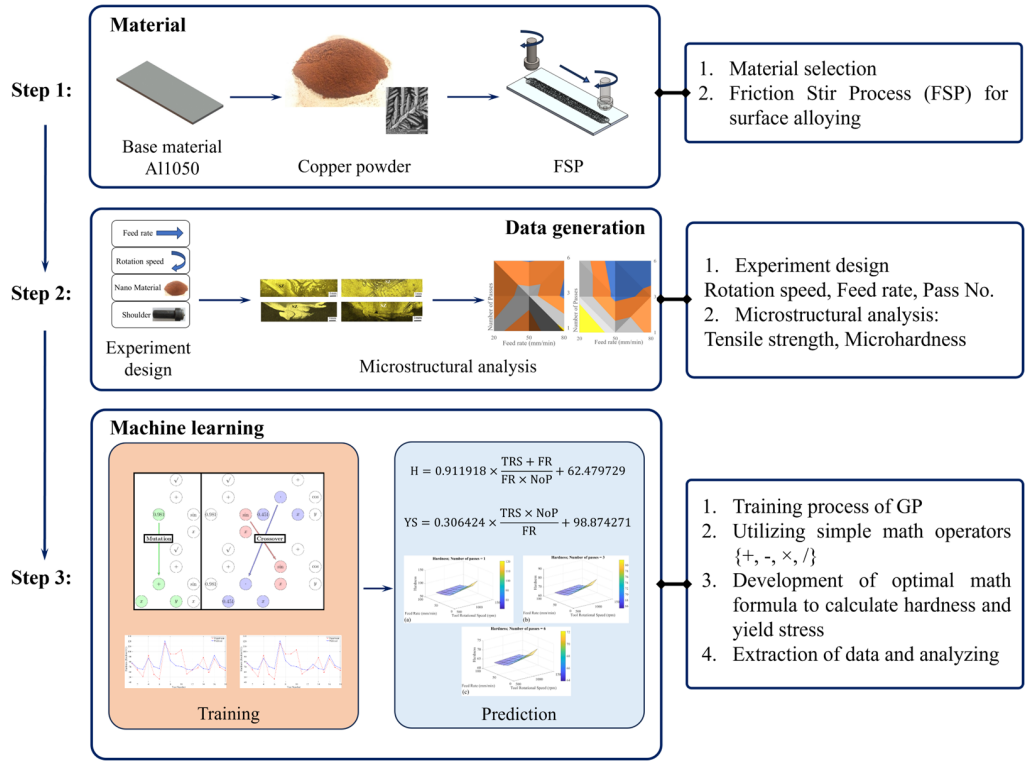

Figure 1. The graphical representation of the proposed method in this study.

2. Materials and Methods

The base metal used in this study was an Al1050 sheet with a thickness of 5 mm. The chemical composition of the base metal can be found in Table 1, while Table 2 presents its mechanical properties.

Table 1. Chemical composition of the Al1050 (wt.%).

Si	Fe	Mn	P	V	Ti	Al
0.071	0.175	0.008	0.004	0.019	0.004	>99.7

Table 2. Mechanical properties of the Al1050 [22].

Tensile Strength	Hardness (Brinell)	Elongation A	Density	Modulus of Elasticity
105–145 MPa	34 HB	12 Min %	2.71 kg/m^3	71 GPa

Cu was employed as the alloying powder for the friction stir processing, which aimed to create a surface alloy. The SEM Image of the Cu powder and the corresponding EDS analysis are presented in Figure 2. The copper powder consisted of 10 ± 0.5 µm particles of 99.8% pure copper Cu. Several variants of friction stir processing exist, including the hole method, groove method, sandwich method, and directed FSP [22]. In this paper, the groove method was utilized. A groove with a depth of 2.5 mm and a width of 1 mm was machined on the aluminum surface, parallel to the rolling direction. The Cu powder was then introduced into the groove, and the groove surface was covered using a pinless tool. The process is carried out using a universal milling machine.

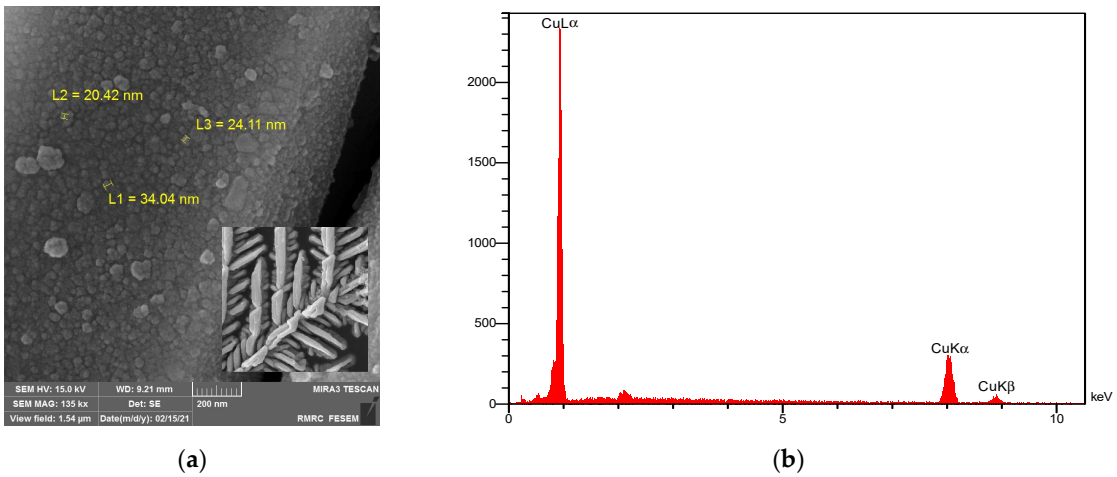

(**a**) (**b**)

Figure 2. Cu powder: (**a**) SEM image of the used reinforcing Cu powder; (**b**) EDS analysis of the reinforcing powder.

A cylindrical pin tool was employed to blend the powder and stir it within the matrix. The dimensions of the equipment can be found in Figure 3a,b. FSP was carried out using a cylindrical pin of 5 mm in diameter and 3 mm in height, along with a shoulder of 16 mm diameter. The FSP zone in both the metallography and tensile specimens are also presented in Figure 3c.

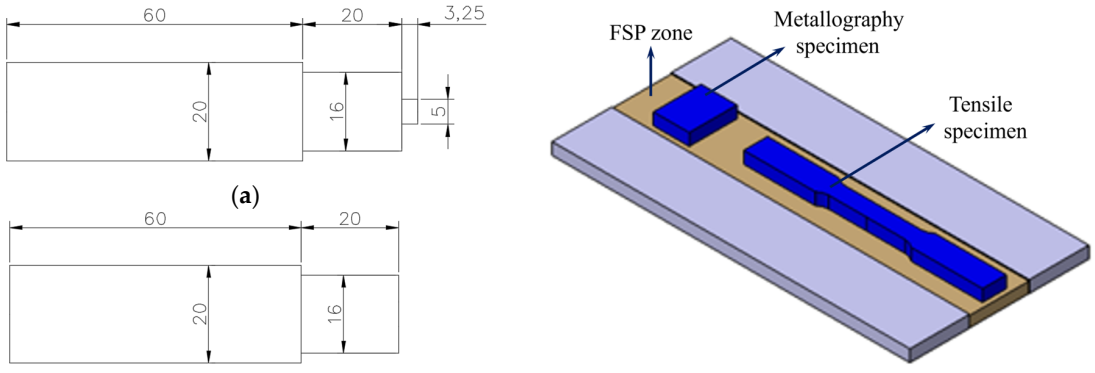

(**a**) (**b**) (**c**)

Figure 3. The tools used for the process and schematic of processed sample: (**a**) detailed dimensions of the friction stir processing tool; (**b**) detailed dimensions of the pinless tool; (**c**) locations where metallography and tensile test specimens were extracted, (all dimensions are in mm).

To avoid excessive penetration of the FSP tool into the workpiece caused by additional heating and plasticization, the plunging force was carefully adjusted. A plunging force of 12 kN was specifically employed to maintain a stable FSP. After each pass, the rotational direction of the welding tool was changed, and the specimen was cooled to room temperature. The investigated parameters in this study were the tool rotation speed, feed rate, and the number of passes, as presented in Table 3. The rest of the process parameters remained constant for all specimens. A tool tilt angle of 3° and shoulder plunge depth of 0.3 mm were used for all specimens.

Table 3. The experiment design.

No.	Tool Rotation Speed (rpm)	Feed Rate (mm/min)	Number of Passes	Hardness	Strength (MPa)
1	1250	80	1	77	94
2	1250	80	3	64	103
3	1250	80	6	51	120
4	1250	50	1	92	111
5	1250	50	3	55	134
6	1250	50	6	46	166
7	1250	20	1	115	98
8	1250	20	3	95	181
9	1250	20	6	95	192
10	630	80	1	103	87
11	630	80	3	56	98
12	630	80	6	64	110
13	630	50	1	68	130
14	630	50	3	88	112
15	630	50	6	59	123
16	630	20	1	85	87
17	630	20	3	69	149
18	630	20	6	63	160

To analyze the mechanical properties of the samples, tensile and microhardness tests were carried out. Longitudinal tensile specimens were fabricated by ASTM-E08 standards [23]. The tensile test was performed using the Sanctum machine with a by Zwick-Roell GmbH & Co. KG, Ulm, Germany, following the ASTM-E08 guidelines, with a tensile speed of 1 mm/min. The strength of the alloyed samples is presented in Table 3.

Table 3 presents the average mechanical properties of the metal within the stir zone, including ultimate tensile strength (UTS) and mean stir zone microhardness. For each set of parameters, three specimens were tested to determine the ultimate tensile strength, and the mean value is reported in Table 3. Microhardness testing was conducted using the Mega Vickers test machine with a 100 g load. To ensure consistency, microhardness measurements were taken at seven points by indenting across the stir zone and along the RS-to-AS midline for each sample, as depicted in Figure 4.

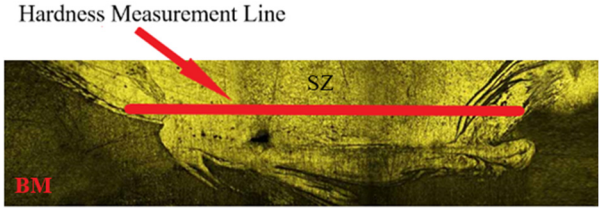

Figure 4. Schematic line depicting the path for microhardness measurements across the cross-section of processed samples.

The reported microhardness value in Table 3 represents the average of these measurements. Figure 4 illustrates the typical measurement path used for all specimens. An OLYMPUS optical microscope was employed to analyze the microstructure evolution of the samples.

The machine learning methodology employed in this study utilizes Genetic Programming (GP), a symbolic optimization technique. GP is an evolutionary computation method that uses a tree representation for potential solutions, which can represent computer programs, mathematical equations, or complex process models. While the details of the GP algorithm are well-known, we focus on key aspects in this paper. This study employs the standard GP algorithm, primarily using arithmetic operations and mathematical functions for model representation.

In GP, models are represented by organized trees containing functions and terminals. Functions are chosen from a predefined set of operators, while terminals are selected from a set of arguments. For linear-in-parameters models, terminals exclude parameters and only include variables. GP population individuals represent nonlinear functions, and parameters are later assigned using the Orthogonal Least Squares (OLS) algorithm. The OLS algorithm efficiently identifies important terms in a linear-in-parameters model by computing error reduction ratios.

The GP fitness function evaluates potential solutions based on their accuracy in fitting the data, often using mean square error (MSE) or correlation coefficients. To balance model complexity and accuracy, a penalty term is incorporated into the fitness function. This penalty discourages overly complex models and promotes simplicity. Additionally, "tree pruning" is used to manage model complexity. GP-generated trees are decomposed into function terms, and lower significant terms are eliminated using error reduction ratios, resulting in simpler, more interpretable models while preserving the overall tree structure. The pruning process can be adjusted with an error reduction ratio threshold to control simplification levels. This methodology combines GP with OLS and tree pruning to enhance the quality and interpretability of generated models.

The parameters for the GP model are carefully selected to balance complexity, computational feasibility, and effective solution space exploration. Table 4 presents the selected parameters, ensuring robustness and reliability in both hardness and ultimate tensile stress prediction models:

Table 4. The hyperparameters of GP for prediction of hardness and strength.

Parameter	Value	Description
Functions	{'+', '*', '/'}	Basic arithmetic operations used to build the GP model equations
Terminals	{'x1′, 'x2′, 'x3′}	Input variables representing features of the dataset
Population size	40	Number of individual programs (models) in the population
Maximum tree depth	50	Maximum depth of the tree structures representing the GP models
Crossover probability	0.8	Probability of combining two parent models to create offspring
Mutation probability	0.7	Probability of randomly altering parts of a model
Selection pressure	0.3	Controls the likelihood of selecting fitter individuals for reproduction
Maximum generations	20	Number of generations (iterations) the GP algorithm runs
Initial temperature	2	Used in simulated annealing processes (if applicable)
Cooling rate	1	Parameter for simulated annealing to reduce the temperature over time (if applicable)
Subpopulation size	30	Size of subpopulations in the algorithm
Tolerance	0.05	Tolerance level for the stopping criterion

Functions: {'+', '*', '/'}—Basic arithmetic operations provide a versatile foundation for constructing complex mathematical models while maintaining simplicity.

Terminals: {'x1', 'x2', 'x3'}—Correspond to the input features of the dataset, ensuring the model utilizes all available information for prediction.

Population size: 40—Balances computational efficiency and genetic diversity, fostering varied evolutionary paths without excessive computational costs.

Maximum tree depth: 5—Controls model complexity, allowing for sufficient depth to capture nonlinear relationships without overfitting.

Crossover probability: 0.8—Promotes combining existing solutions, potentially yielding better offspring models.

Mutation probability: 0.7—Introduces significant variation into the population, preventing premature convergence and encouraging the exploration of the solution space.

Selection pressure: 0.3—Balances selecting the best models for reproduction with maintaining diversity by occasionally selecting less fit models, facilitating broader solution exploration.

Generations: 20—Provides sufficient time for the population to evolve and improve, considering computational constraints.

Simulated annealing (if applied):

- Initial temperature: 2
- Cooling rate: 1—Controls the acceptance of worse solutions initially, avoiding local optima and gradually reducing acceptance to promote convergence.

Subpopulation size: 30—Enhances diversity within the overall population, leading to more varied and potentially better solutions through different evolutionary paths.
Tolerance level: 0.05—Ensures the algorithm halts when improvements in the models become minimal, saving computational resources while maintaining solution quality.

These parameters ensure robustness and reliability in the GP approach, effectively balancing complexity, computational feasibility, and optimal solution search.

3. Results and Discussions

Friction stir alloying (FSA) is an innovative technique that has garnered considerable attention in the field of materials science and engineering. This study investigates the friction stir alloying of Al1050 with Cu powder. The findings are presented and discussed in two main sections. The first section discusses the experimental results, while the second section describes the employed machine learning method.

3.1. Experimental Results

Friction stir alloying has demonstrated successful application across various alloys, such as aluminum-based alloys, magnesium alloys, and titanium alloys [22]. The present investigation adds Cu powder to an Al1050 aluminum sheet. FSA enhances material properties such as microhardness and tensile strength. Additionally, FSA has shown promise in improving corrosion resistance by creating a more homogeneous distribution of alloying elements. One major limitation is the difficulty in achieving a uniform distribution of alloying elements throughout the entire material during processing. This issue can lead to localized variations in mechanical properties and hinder widespread industrial adoption.

Figure 5 presents the cross-sections of four processed specimens, specifically specimens 3, 5, 6, and 7.

In the cross-section of the friction stir alloyed specimens, different zones, including the thermomechanically affected zone (TMAZ), stir zone (SZ), heat affected zone (HAZ), and base metal (BS), can be detected. Figure 6 presents different zones on the microstructure of the alloyed specimens. The solution of copper particles also is evident in the cross-section, which indicates the success of the alloying process. However, in some cases, a big agglomerated Cu powder could be detected, an example of which is presented in Figure 7.

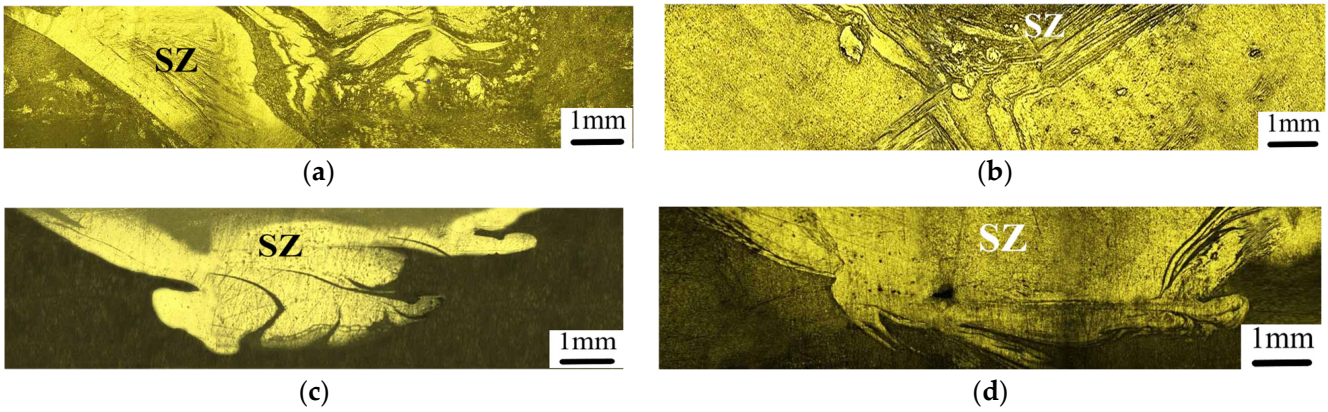

Figure 5. Macrographs of a cross-section of proceeds specimens: (**a**) specimen No. 3; (**b**) specimen No. 5; (**c**) specimen No. 6; (**d**) specimen No. 7.

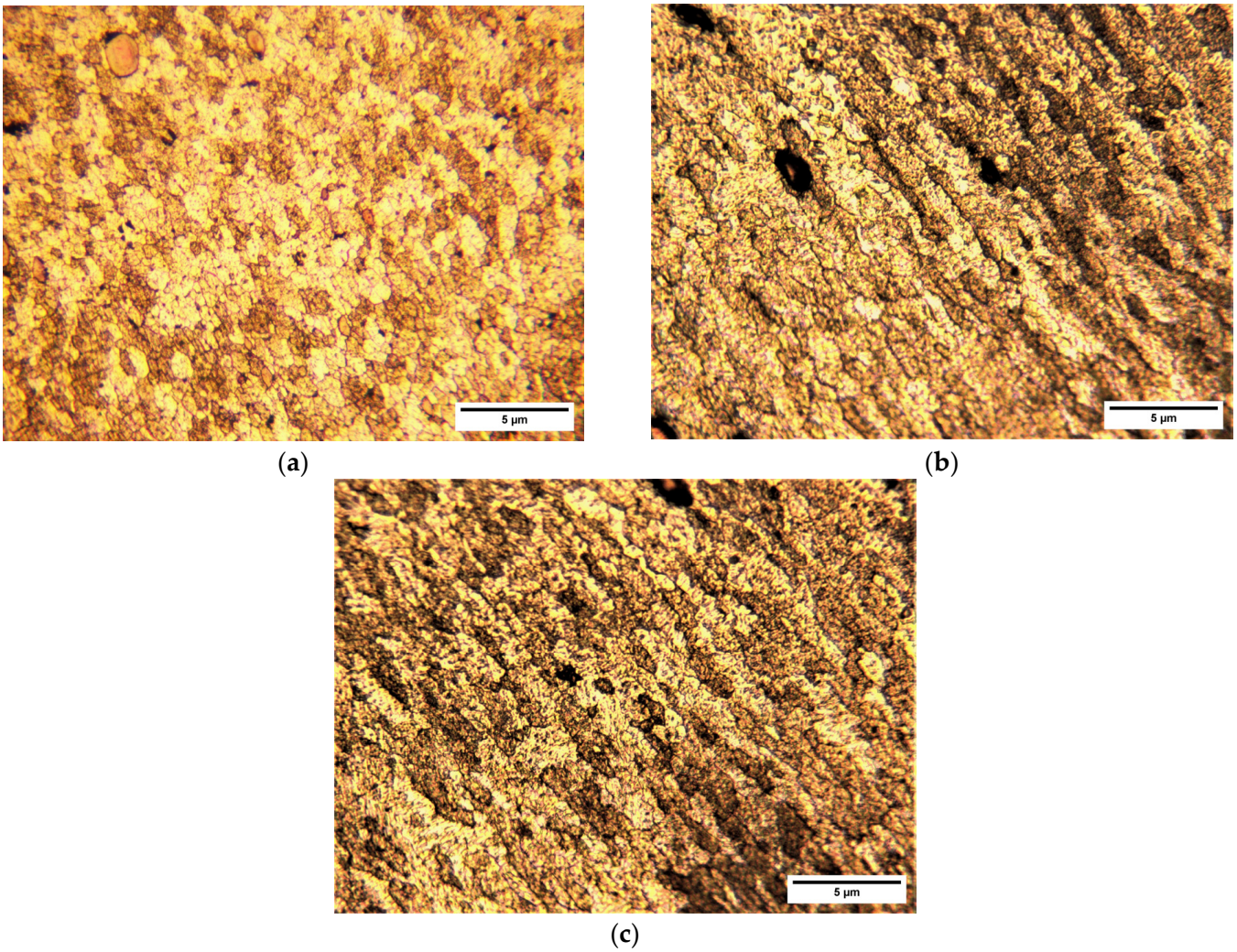

Figure 6. Various zones in the cross-section of friction stir processed specimen No. 3 (**a**) stir zone; (**b**) thermomechanically affected zone; (**c**) heat affected zone.

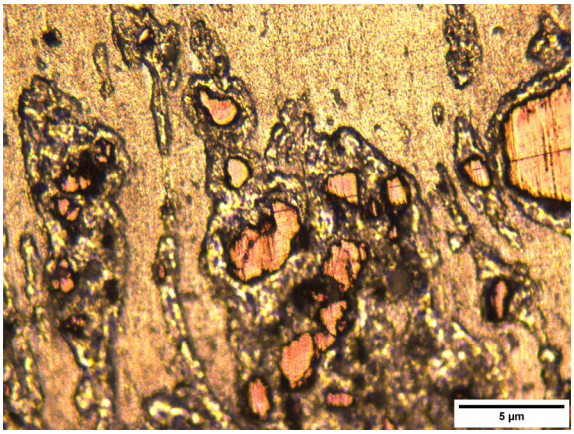

Figure 7. Cu trace on the processed zone of specimen No. 3.

The main question that should be answered is which microstructural factor or factors govern the hardness in the Cu alloyed Al1050, and how does it change when the processing parameters change? According to Figure 8, the effects of processing parameters on the hardness are as follows: in general, it could be said that the higher tool rotation speed results in a higher hardness. As mentioned in the literature, with increasing tool rotational speed, heat input increases, which indicates that recrystallized grains will grow more and the hardness will drop [24,25]. However, in this case, the results are opposite, which could be attributed to the Cu trace and the powder agglomeration. Here, there is another mechanism together with the grain size that affects the hardness, namely powder distribution. With an increase in tool rotation speed, the powder is distributed well and both solution and intermetallic component formation are accelerated, which results in a higher hardness. More passes result in lower hardness. When the specimen is processed in three passes, the total heat input to the processed zone increases, which increases the grain growth. While more passes result in a more homogeneous powder distribution, which is typically assumed to enhance the mechanical properties of the produced surface alloy, this is not always the case. For example, Figure 8 shows that increasing the number of passes often results in a decrease in hardness. This reduction in hardness can be attributed to the higher heat input associated with additional passes, which promotes grain growth and subsequently reduces hardness.

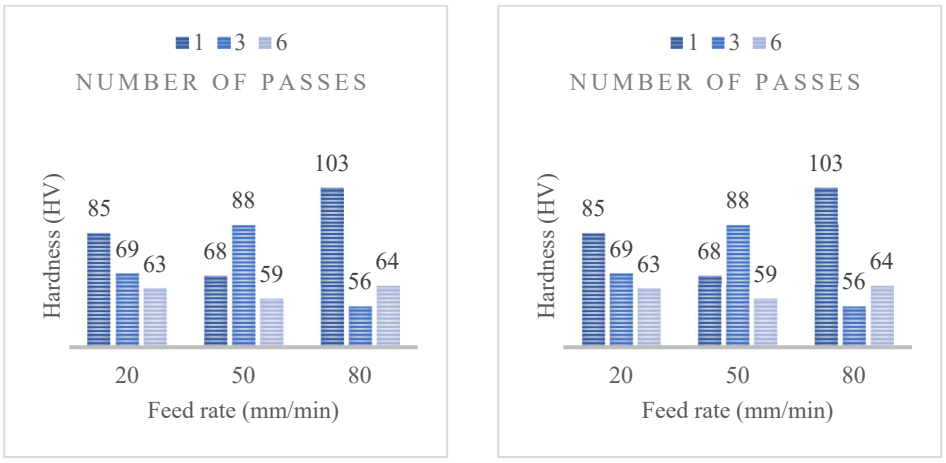

(**a**) (**b**)

Figure 8. Hardness of FSPed specimens. For each feed rate, three different specimens processed in three different passes are presented. The microhardness values are in HV: (**a**) processed at a tool rotation speed of 630 rpm; (**b**) processed at a tool rotation speed of 1250 rpm.

In general, it is predicted that any increase in the feed rate results in an increase in hardness. This is because an increase in feed rate means lower heat input to the alloyed zone, resulting in limited grain growth [26,27]. However, as presented in Figure 8, the hardness changes in some cases deviate from this general behavior. This discrepancy can be explained by powder agglomeration, which occurs when the feed rate is high. The increase in pass number results in a strength increase. A higher pass number means more powder distribution and a more homogenous microstructure, which is one reason for an alloy to have a higher strength. The strength of the base metal is 115 MPa, which could be increased by the surface alloying procedure up to 192 MPa. Any decrease in the feed rate results in an increase in strength. When the feed rate decreases, the alloying zone is subjected to heat and mechanical work for a longer time, which provides enough time for the diffusion and formation of hard IMCs, which are the main reason for the increasing strength in aluminum alloys. Any increase in the tool's rotation speed results in an increase in strength. Again, this is the opposite result of the alloying procedure in comparison to the welding. In the welding of aluminum alloys, any increase in the tool rotation speed while providing more heat results in a bigger grain size and solution of hard carbides, which decreases the strength of the specimen. However, in the present study, because it involves alloying in this case, increasing the tool rotation speed accelerates the alloying procedure and the formation of hard IMCs, which increase the strength of the produced alloy. The variation in the strength of the produced alloy versus processing parameters is presented in Figure 9.

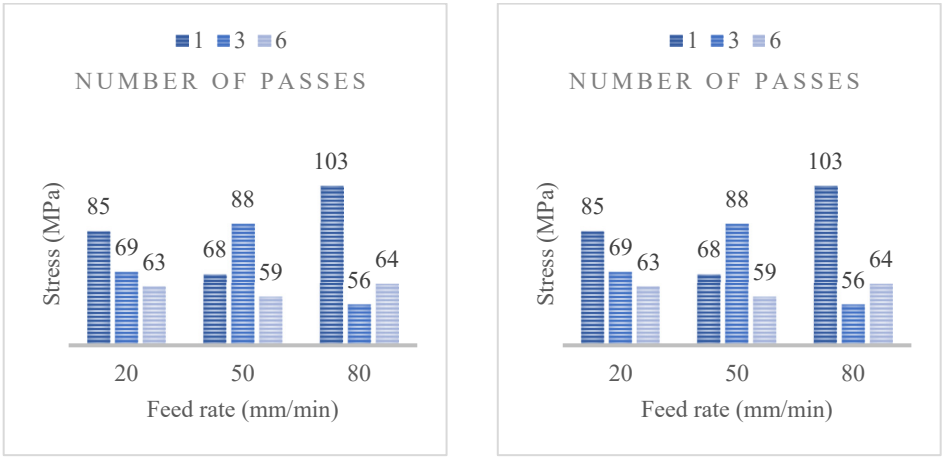

Figure 9. Tensile strength of FSPed specimens. For each feed rate, three different specimens processed in three different passes are presented. The strength values are in MPa: (**a**) processed at a tool rotation speed of 630 rpm; (**b**) processed at a tool rotation speed of 1250 rpm.

3.2. Machine Learning Results

The proposed methodology in the previous section is implemented using MATLAB R2022a software under the freely provided Toolbox [28]. After the implementation of the proposed method, the functions below are extracted to calculate hardness and ultimate tensile stress based on the process input parameters, including tool rotation speed (rpm), feed rate (mm/min), and number of passes. The dataset is divided into 13 and 5 (out of 18, as shown in Table 3) for the purpose of training and testing of the proposed GP. The following formulas are extracted as a mathematical way to calculate the hardness and stress using every possible process parameter as follows:

$$\text{Hardness} = 0.91 \times \frac{\text{Tool rotation speed} + \text{Feed rate}}{\text{Feed rate} \times \text{Number of passes}} + 62.48$$

$$\text{Stress} = 0.31 \times \frac{\text{Tool rotation speed} \times \text{Number of passes}}{\text{Feed rate}} + 98.87$$

The regression plot during the training/testing process of the methodology is shown in Figure 10 for the prediction of hardness and tensile stress. Based on the represented results on Figure 10a, the R^2 between the observed and predicted hardness during the training and testing process of the proposed GP are 0.5277 and 0.1633, respectively. Also, Figure 10b shows that the R^2 between the observed and predicted tensile stress are 0.7621 and 0.7288, respectively.

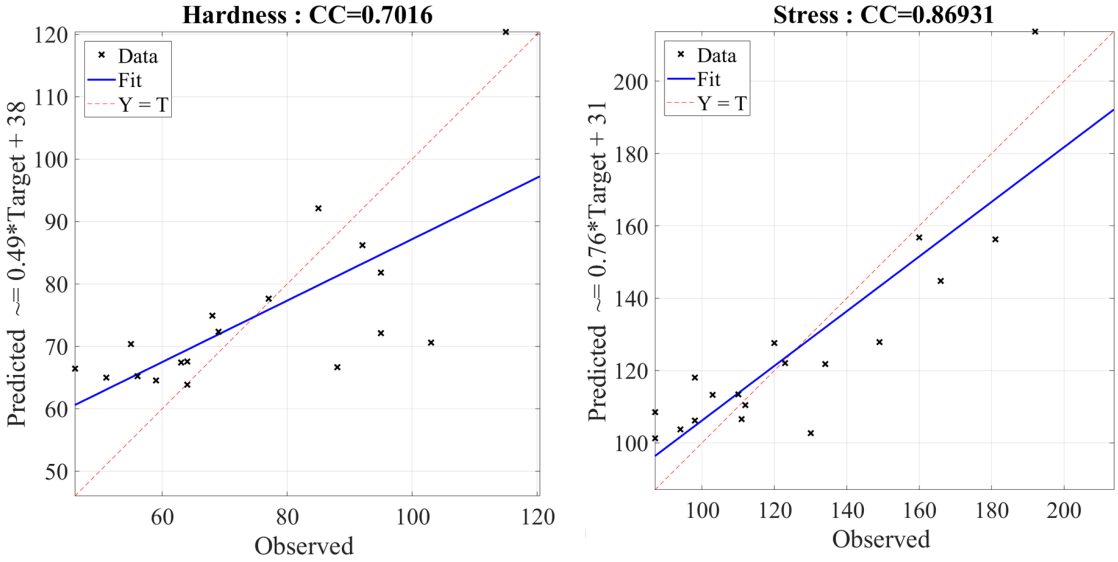

(**a**) (**b**)

Figure 10. The regression of the proposed methodology during the training/testing process for prediction of: (**a**) hardness; (**b**) tensile stress.

Figure 11 shows the experimentally recorded and predicted hardness and tensile stress of the final products of the friction stir alloying. Based on the represented results in Figure 11a, the CC between the experimentally recorded and predicted hardness of the final FSA products is 0.7016. In addition, Figure 11b shows that the CC between the experimentally recorded and predicted hardness of the final FSA products is 0.8693.

(**a**)

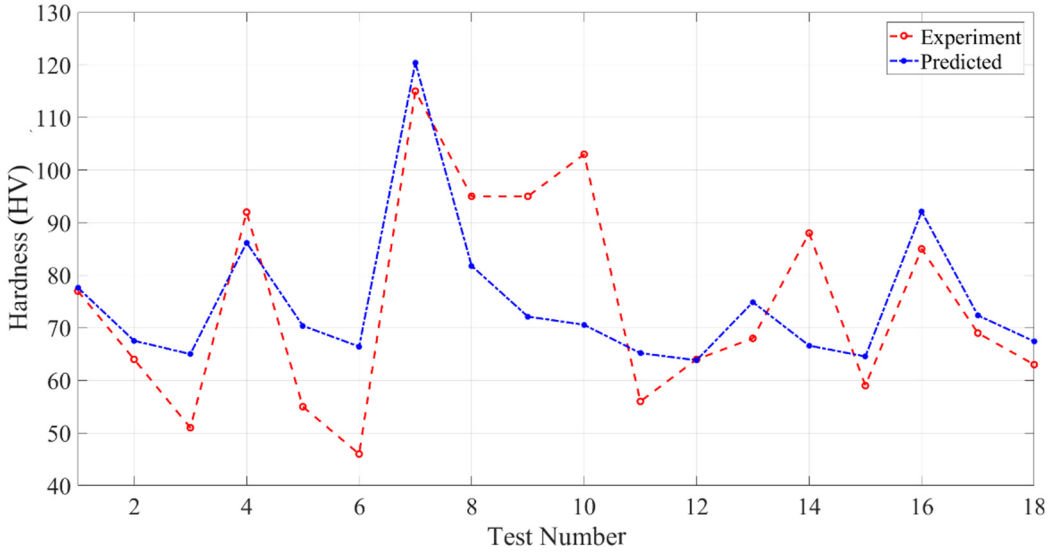

Figure 11. *Cont.*

(**b**)

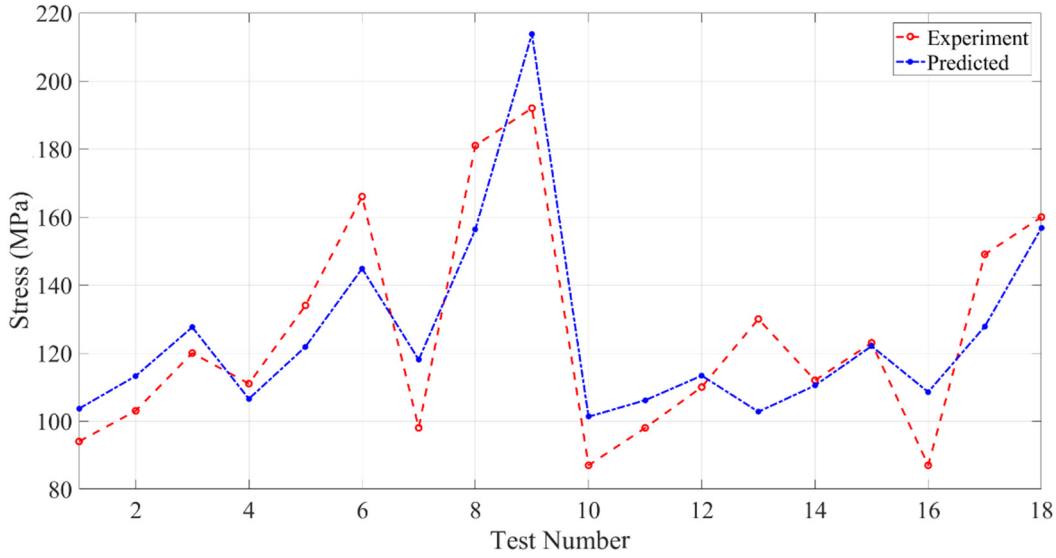

Figure 11. The experimental recorded dataset and predicted ones using: (**a**) GP hardness; (**b**) GP tensile stress.

Figure 12 shows the error between the experimentally recorded and predicted hardness and tensile stress of the FSA final products. Based on the represented results in Figure 12a, MAE, MSE, and RMSE, the experimentally recorded and predicted hardness of the final FSA products are 10.65, 1.88, and 13.70, respectively. In addition, Figure 12b shows that the MAE, MSE, and RMSE between the experimentally recorded and predicted hardness of the final FSA products are 12.95, 2.39, and 15.47, respectively.

(**a**)

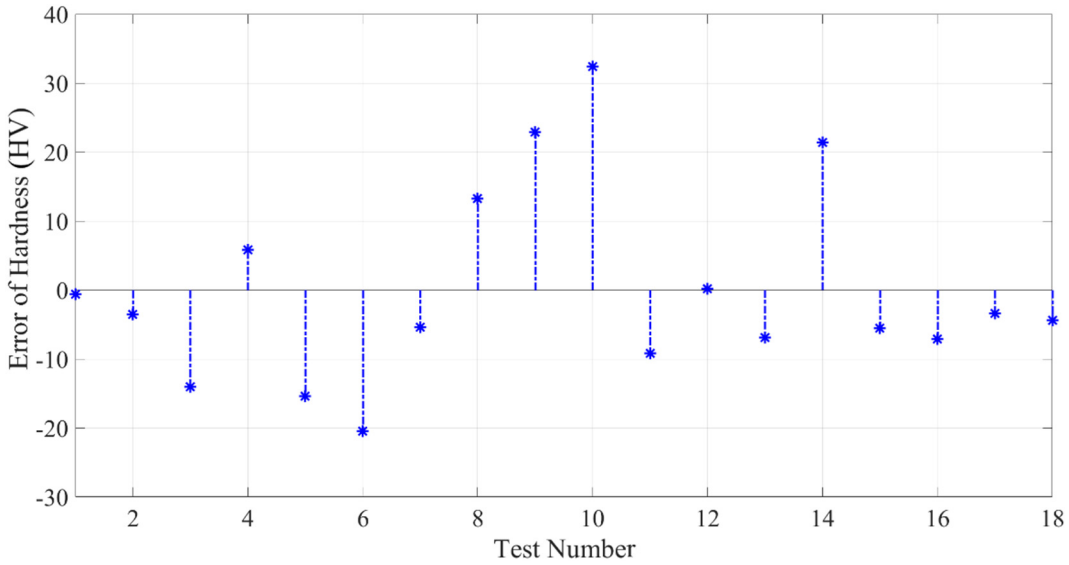

Figure 12. *Cont.*

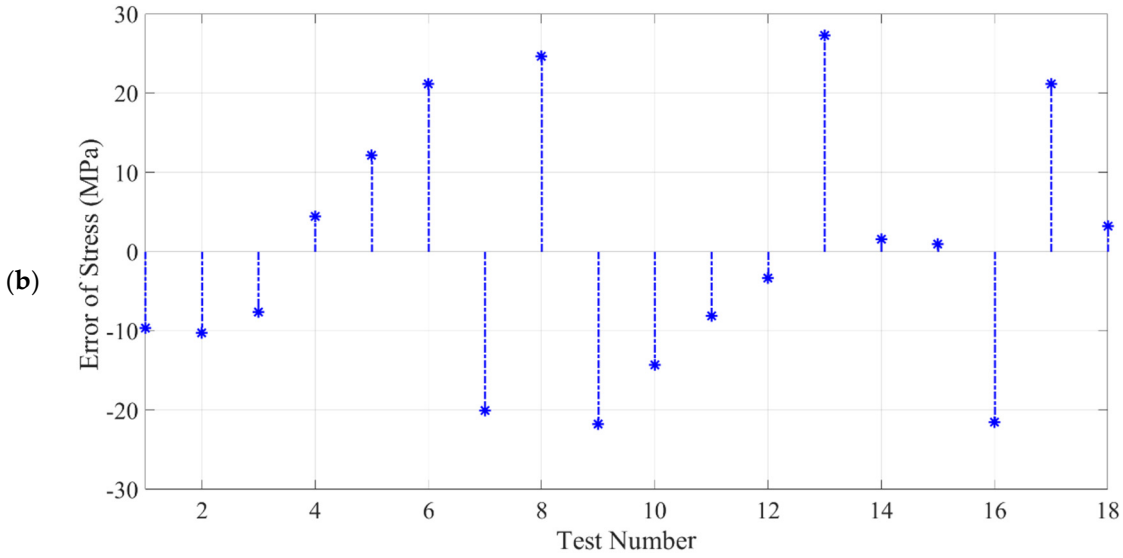

Figure 12. The error between the experimental recorded dataset and predicted ones using: (**a**) GP hardness; (**b**) GP tensile stress.

Finally, the variation in hardness and tensile stress based on the extracted formulas by GP based on the different number of passes are shown in Figures 13 and 14, respectively.

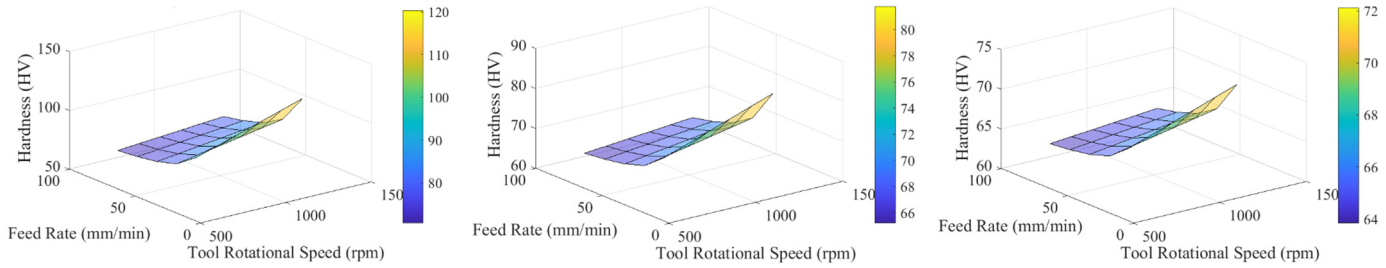

Figure 13. The variation in hardness under different tool rotation speeds (rpm) and feed rates (mm/min): (**a**) number of passes = 1; (**b**) number of passes = 3; (**c**) number of passes = 6.

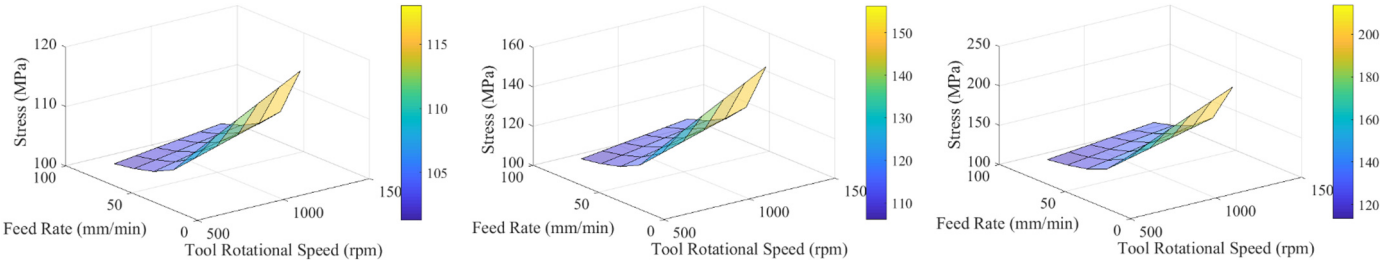

Figure 14. The variation in tensile stress (MPa) under different tool rotation speeds (rpm) and feed rates (mm/min): (**a**) number of passes = 1; (**b**) number of passes = 3; (**c**) number of passes = 6.

4. Conclusions

In conclusion, this study underscores the effectiveness of friction stir processing in fabricating a surface alloy with Cu powder, showcasing notable improvements in the mechanical properties of the Al1050 aluminum alloy. By investigating various parameters such as tool rotation speed, feed rate, and the number of passes, we have gained insights into the

microstructural evolution and mechanical behavior of the resulting surface alloy. The initial non-uniform stir zone was successfully homogenized with subsequent passes, facilitating the compaction of copper particles and their integration with aluminum. This process led to a significant enhancement in the strength of the base metal, attributed to both the presence of copper and the refinement of grain size post-alloying. Moreover, integrating machine learning techniques has further enriched our understanding of friction stir processing for surface alloying applications. Specifically, Genetic Programming was adeptly employed to model the intricate relationship between processing parameters and mechanical properties, offering predictive capabilities for optimizing the surface alloying process. By leveraging machine learning, we have deepened our insights into the underlying mechanisms governing alloy formation and streamlined the process optimization efforts. In summary, these findings mark a significant stride in materials science and engineering, providing valuable insights into developing high-performance surface alloys for diverse industrial applications. Notably, utilizing machine learning techniques offers a promising avenue for future research and development endeavors, paving the way for enhanced efficiency and precision in alloy design and fabrication processes. Here are the main findings:

- Increasing the tool rotation speed leads to higher hardness.
- A greater number of passes results in lower hardness.
- Increasing the feed rate leads to a decrease in hardness.
- The strength increases with an increase in the number of passes.
- Decreasing the feed rate results in higher strength.
- Increasing the tool rotation speed leads to higher strength.
- The base metal has a strength of 115 MPa, but it can be increased to 192 MPa through the surface alloying process.
- The system's real-time capabilities ensure the effective identification of material defects during live production processes.

Author Contributions: S.P. (Siamak Pedrammehr) Conceptualization, Software, Data curation, Validation, Methodology, Investigation, Writing—original draft, review, and editing. M.S., K.I.A.-L.A.-A., S.P. (Sajjad Pakzad), A.Z.J. Administration, Conceptualization, Data curation, Methodology analysis, Formal analysis, Writing—original draft. M.M.E. Administration, Conceptualization, Supervision, Methodology analysis, writing—review and editing. M.R.C.Q. Software, Data curation, Validation, Methodology, Investigation, review, and editing. All authors have read and agreed to the published version of the manuscript.

Funding: This research received no external funding.

Data Availability Statement: Data will be made available on request.

Conflicts of Interest: The authors declare that they have no known competing financial interests or personal relationships that could have appeared to influence the work reported in this paper.

References

1. Gan, Y.; Solomon, D.; Reinbolt, M. Friction Stir Processing Of Particle Reinforced Composite Materials. *Materials* **2010**, *1*, 329–350. [CrossRef]
2. Hasan, M.; Tolba, S.; Allam, N. In Situ Formation Of Graphene Stabilizes Zero-valent Copper Nanoparticles and Significantly Enhances The Efficiency Of Photocatalytic Water Splitting. *ACS Sustain. Chem. Eng.* **2018**, *12*, 16876–16885. [CrossRef]
3. Sajed, M.; Seyedkashi, S.H. Solid-state local micro-alloying of thick ST37 steel plates with SiC powder using a modified friction hydro-pillar process. *J. Mater. Res. Technol.* **2020**, *9*, 7158–7171. [CrossRef]
4. Adetunji, O.R.; Olukuade, M.L.; Simka, W.; Sowa, M.; Adesusi, O.M.; Okediran, I.K. Production and Characterization of Amorphous Aluminum-Copper Alloy for Aerospace Applications. *Eur. J. Eng. Technol. Res.* **2017**, *2*, 1–5.
5. Stojanovic, B.; Bukvic, M.; Epler, I. Application of Aluminum and Aluminum Alloys in Engineering. *Appl. Eng. Lett. J. Eng. Appl. Sci.* **2018**, *3*, 52–62. [CrossRef]
6. Lequeu, P.; Smith, K.P.; Daniélou, A. Aluminum-Copper-Lithium Alloy 2050 Developed for Medium to Thick Plate. *J. Mater. Eng. Perform.* **2010**, *19*, 841–847. [CrossRef]
7. Chainarong, S.; Muangjunburee, P.; Suthummanon, S. Friction Stir Processing Of SSM356 Aluminium Alloy. *Procedia Eng.* **2014**, *97*, 732–740. [CrossRef]

8. Liu, L.; Nakayama, H.; Fukumoto, S.; Yamamoto, A.; Tsubakino, H. Microscopic Observations of Friction Stir Welded 6061 Aluminum Alloy. *Mater. Trans.* **2004**, *2*, 288–291. [CrossRef]
9. Eslami, N.; Harms, A.; Deringer, J.; Fricke, A.; Böhm, S. Dissimilar Friction Stir Butt Welding Of Aluminum and Copper With Cross-section Adjustment For Current-carrying Components. *Metals* **2018**, *9*, 661. [CrossRef]
10. Uematsu, Y.; Tozaki, Y.; Tokaji, K.; Nakamura, M. Fatigue Behavior Of Dissimilar Friction Stir Welds Between Cast and Wrought Aluminum Alloys. *Strength Mater.* **2008**, *1*, 138–141. [CrossRef]
11. Shafiei-Zarghani, A.; Kashani-Bozorg, S.F.; Zarei-Hanzaki, A. Microstructures and mechanical properties of Al/Al_2O_3 surface nano-composite layer produced by friction stir processing. *Mater. Sci. Eng. A* **2009**, *500*, 84–91. [CrossRef]
12. Huang, C.; Aoh, J. Friction Stir Processing Of Copper-coated SiC Particulate-reinforced Aluminum Matrix Composite. *Materials* **2018**, *4*, 599. [CrossRef]
13. Sharma, D.; Patel, V.; Badheka, V.; Mehta, K.; Upadhyay, G. Different Reinforcement Strategies of Hybrid Surface Composite AA6061/(B4C+MoS_2) Produced By Friction Stir Processing. *Materwiss. Werksttech.* **2020**, *11*, 1493–1506. [CrossRef]
14. Wang, T.; Shukla, S.; Gwalani, B.; Sinha, S.; Thapliyal, S.; Frank, M.; Mishra, R.S. Co-introduction of precipitate hardening and TRIP in a TWIP high-entropy alloy using friction stir alloying. *Sci. Rep.* **2021**, *11*, 1579. [CrossRef] [PubMed]
15. Rubtsov, V.; Chumaevskii, A.; Gusarova, A.; Knyazhev, E.; Gurianov, D.; Zykova, A.; Tarasov, S. Macro-and Microstructure of In Situ Composites Prepared by Friction Stir Processing of AA5056 Admixed with Copper Powders. *Materials* **2023**, *16*, 1070. [CrossRef]
16. Verma, S.; Msomi, V.; Mabuwa, S.; Merdji, A.; Misra, J.P.; Batra, U.; Sharma, S. Machine learning application for evaluating the friction stir processing behavior of dissimilar aluminium alloys joint. *Proc. Inst. Mech. Eng. Part L J. Mater. Des. Appl.* **2022**, *236*, 633–646. [CrossRef]
17. Verma, S.; Misra, J.P.; Popli, D. Modeling of friction stir welding of aviation grade aluminium alloy using machine learning approaches. *Int. J. Model. Simul.* **2022**, *42*, 1–8. [CrossRef]
18. Chadha, U.; Selvaraj, S.K.; Gunreddy, N.; Sanjay Babu, S.; Mishra, S.; Padala, D.; Shashank, M.; Mathew, R.M.; Kishore, S.R.; Panigrahi, S.; et al. A survey of machine learning in friction stir welding, including unresolved issues and future research directions. *Mater. Des. Process. Commun.* **2022**, *2022*, 2568347. [CrossRef]
19. Anandan, B.; Manikandan, M. Machine learning approach with various regression models for predicting the ultimate tensile strength of the friction stir welded AA 2050-T8 joints by the K-Fold cross-validation method. *Mater. Today Commun.* **2023**, *34*, 105286. [CrossRef]
20. Acharya, M.; Mandal, A. Microstructure Study of Friction Stir Processed Hypereutectic Al-20Si Alloy and Analysis of the Wear Behaviour using Machine Learning Algorithms. *Silicon* **2024**, *16*, 3539–3551. [CrossRef]
21. Elsheikh, A.H. Applications of machine learning in friction stir welding: Prediction of joint properties, real-time control and tool failure diagnosis. *Eng. Appl. Artif. Intell.* **2023**, *121*, 105961. [CrossRef]
22. Iwazesko, J.; Sajed, M. Technological Aspects of Producing Surface Composites by Friction Stir Processing—A Review. *J. Compos. Sci.* **2021**, *5*, 323. [CrossRef]
23. ASTM International. *ASTM E08: Standard Test Methods for Tension Testing of Metallic Materials*; ASTM International: West Conshohocken, PA, USA, 2023.
24. Khan, N.Z.; Mir, M.A.; Maqbool, A.; Khan, H.A. Evolution of Strengthening Precipitates During Friction Stir Welding of Al-Zn and Al-Cu Alloys. *Trans. Indian Inst. Met.* **2024**. [CrossRef]
25. Jamshidi Aval, H.; Galvão, I. Effect of Tool Rotational Speed on Microstructure and Mechanical Properties of Friction Stir Welded Al–16Si–4Cu–10SiC Composite/Al–4Cu–Mg Alloy Joints. *Metallogr. Microstruct. Anal.* **2024**, 1–15. [CrossRef]
26. Elangovan, K.; Balasubramanian, V. Influences of tool pin profile and welding speed on the formation of friction stir processing zone in AA2219 aluminium alloy. *J. Mater. Process. Technol.* **2008**, *200*, 163–175. [CrossRef]
27. Mishra, R.S.; Ma, Z.Y. Friction stir welding and processing. *Mat. Sci. Eng. R.* **2005**, *50*, 1–78. [CrossRef]
28. Abonyi, J. *Genetic Programming MATLAB Toolbox*; MathWorks: Natick, MA, USA, 2023.